Atmospheric
Chemistry
and Physics

Supplement of

Ice crystal number concentration estimates from lidar–radar satellite remote sensing – Part 1: Method and evaluation

Odran Sourdeval et al.

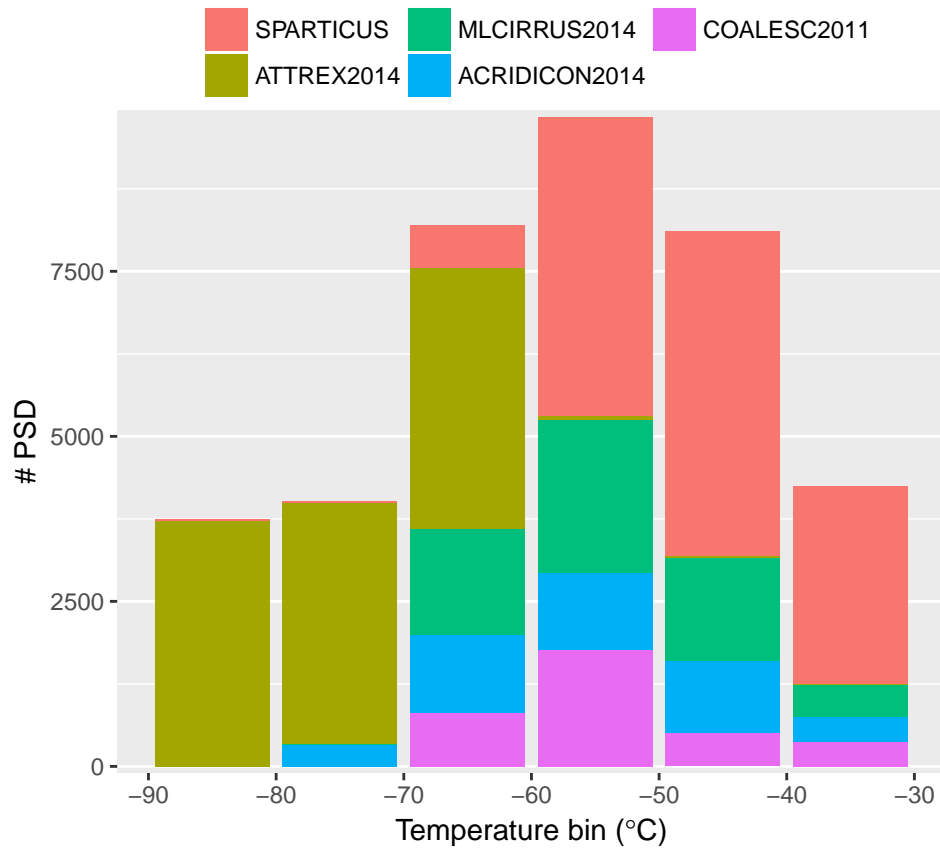*Correspondence to:* Odran Sourdeval (odran.sourdeval@univ-lille.fr)

Figure S1: Stacked histogram showing the distribution of PSDs for each campaign described in Sec. 3.2 (color code above figure) per 10°C bins from -90 to -30°C.
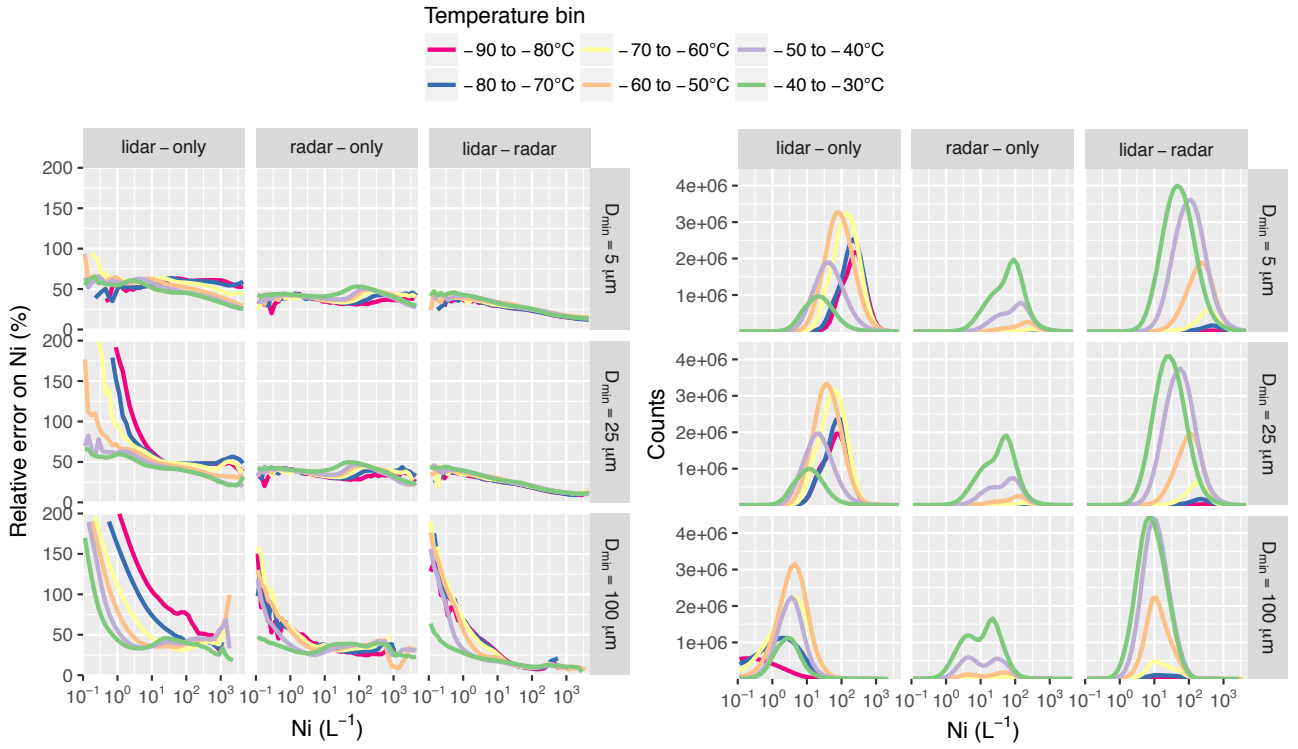
Figure S2: The left figure shows relative errors on DARDAR-Nice N_i estimates obtained by propagating the Gaussian standard-deviations on IWC and N_0^* provided in DARDAR operational retrievals (here based on 500 orbits; Jan-Feb 2008). The propagation method is mentioned in Sec. A2. These errors are provided as function of N_i per temperature bins (color lines), minimum diameter threshold bins for the N_i integration (rows; see Sec. 3.3), and instrumental conditions (columns; see Sec. A1). To clearly identify the dominating errors under different temperature and instrumental conditions, the right figure similarly indicates the distribution of N_i values in each panel.
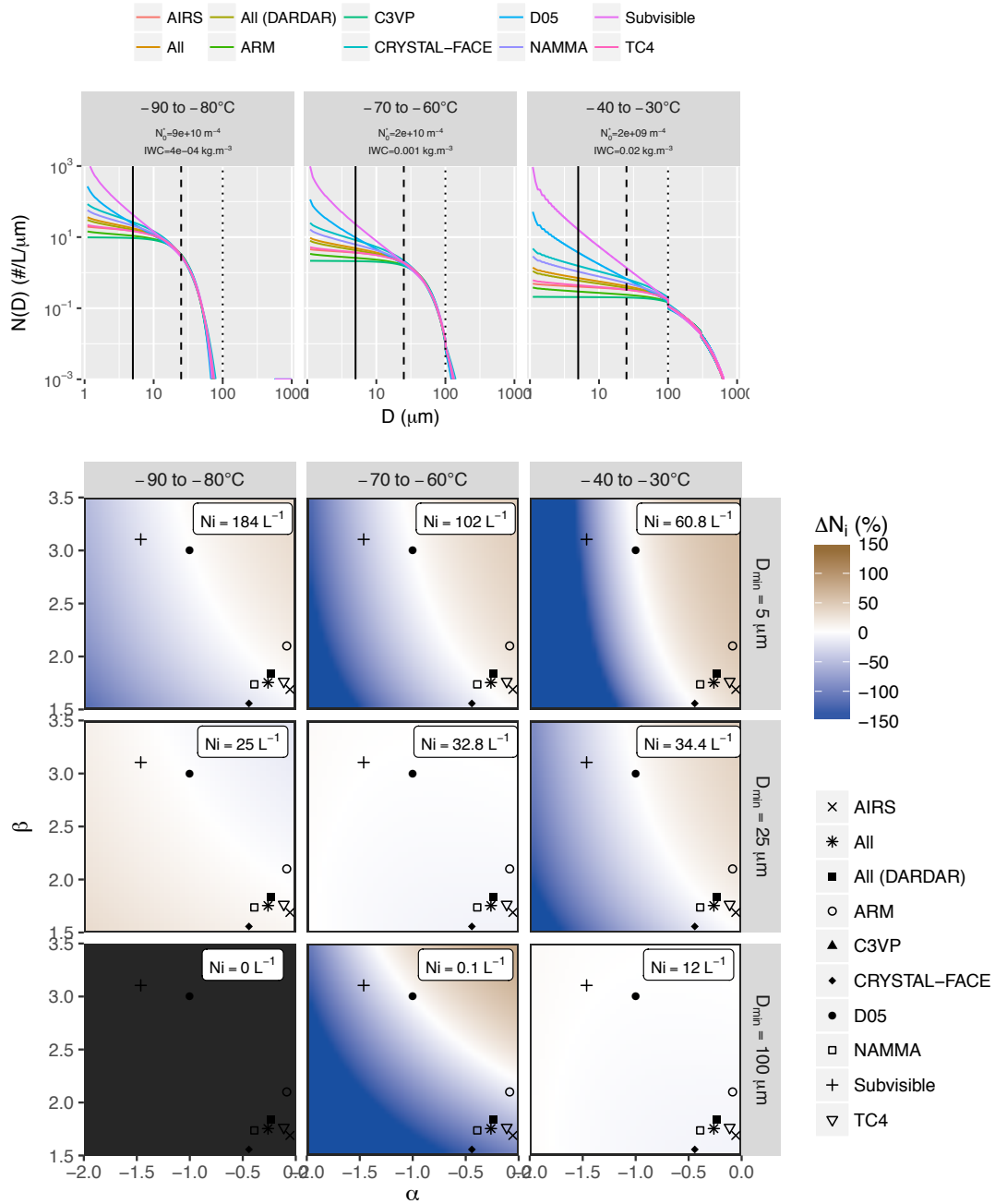
Figure S3: Analysis of the sensitivity of DARDAR-Nice N_i estimates to prior PSD shape assumptions (α and β parameters in Eq. (4)). The top figure shows PSD predictions by the D05 parameterization in 3 temperature bins. For each bin, representative N_0^* and D_m values (indicated in the legend) have been selected based on all in situ campaigns described in Sec. 3.2. The D05 PSD is shown in blue and other colors correspond to PSDs computed using α and β values extracted by Delanoë et al. [2014, D14] from multiple in situ campaigns (see Table 4 of that study or figure below). Vertical plain, dashed and dotted lines indicate the position of $D_{min} = 5$, 25 and 100μm, respectively. The bottom figure indicates relative biases ΔN_i between predictions by D05 (N_{iD05}) and the N_i obtained from a wide range of α (x-axis) and β (y-axis) values. Brown and blue color therefore indicate an overestimation and underestimation of N_i by D05. Specific α and β values from each campaign used in D14 are indicated by various point shapes. D05 is represented by a black dot. ΔN_i is computed for each selected D_{min} threshold (rows; see Sec. 3.3) and per temperature bins (columns) similarly to the top figures. The N_{iD05} values are indicated in each panel.
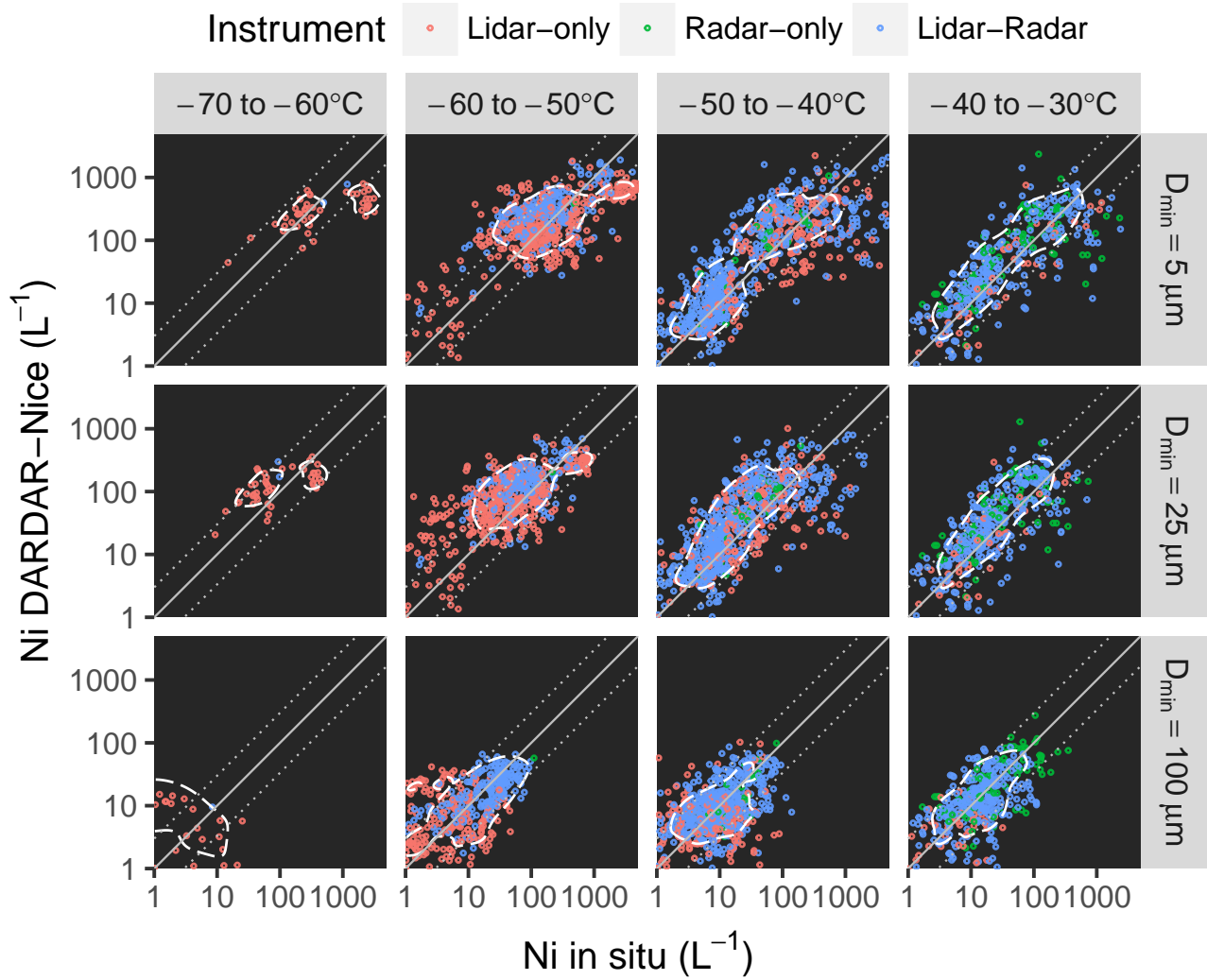
Figure S4: Similar to Fig. 2 of the paper, scatterplots of N_i retrieved by DARDAR-Nice as function of the co-incident 2D-S measurements during SPARTICUS. Red, green and blue dots indicate that N_i estimates were obtained in lidar-, radar-only and lidar-radar conditions. White isolines show the overall 68% confidence interval per D_{min} and T_c bins.
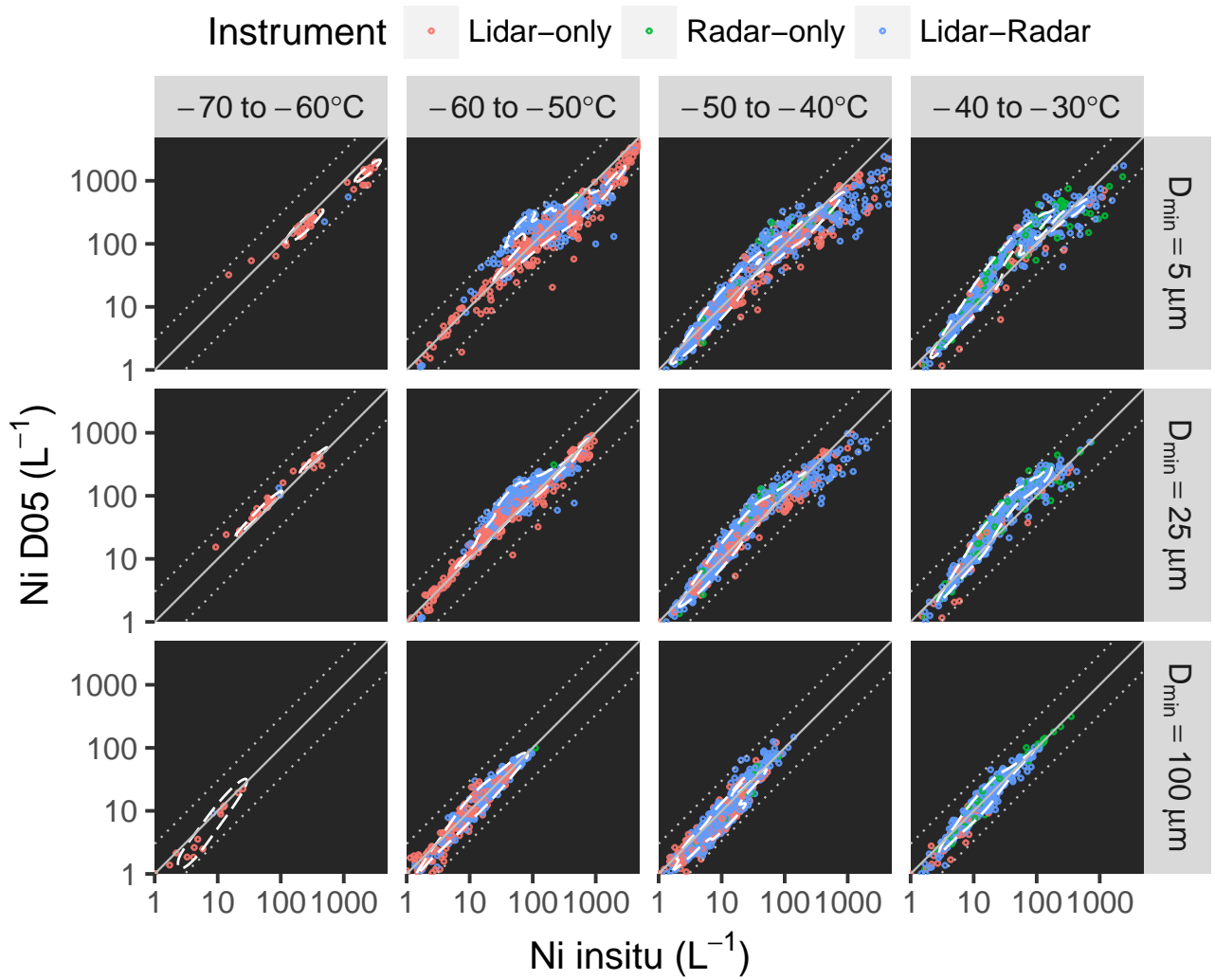
Figure S5: Similar to Fig. S4 but for D05 predictions (based on in situ IWC and N_0^*) as function of 2D-S measurements.
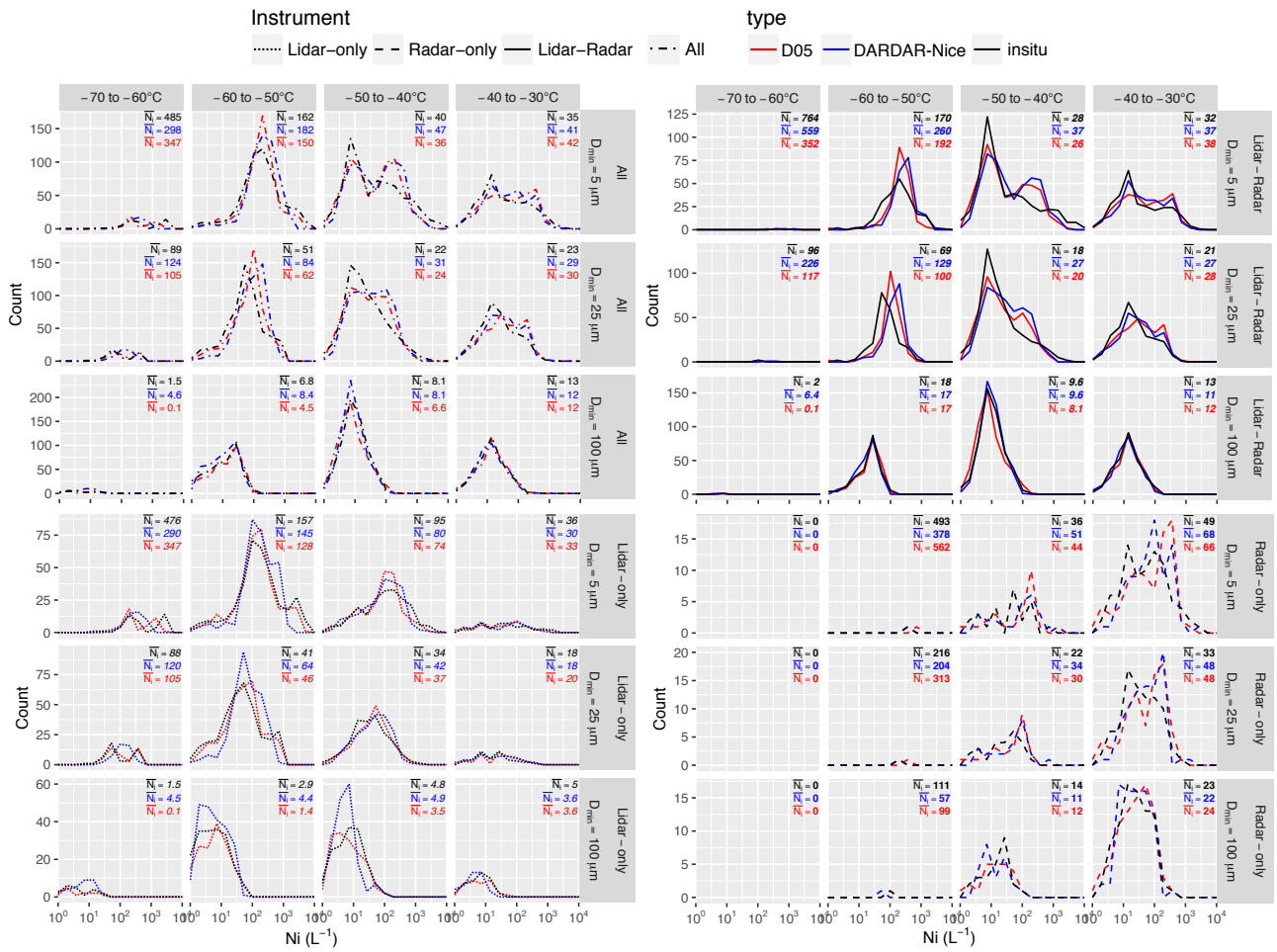
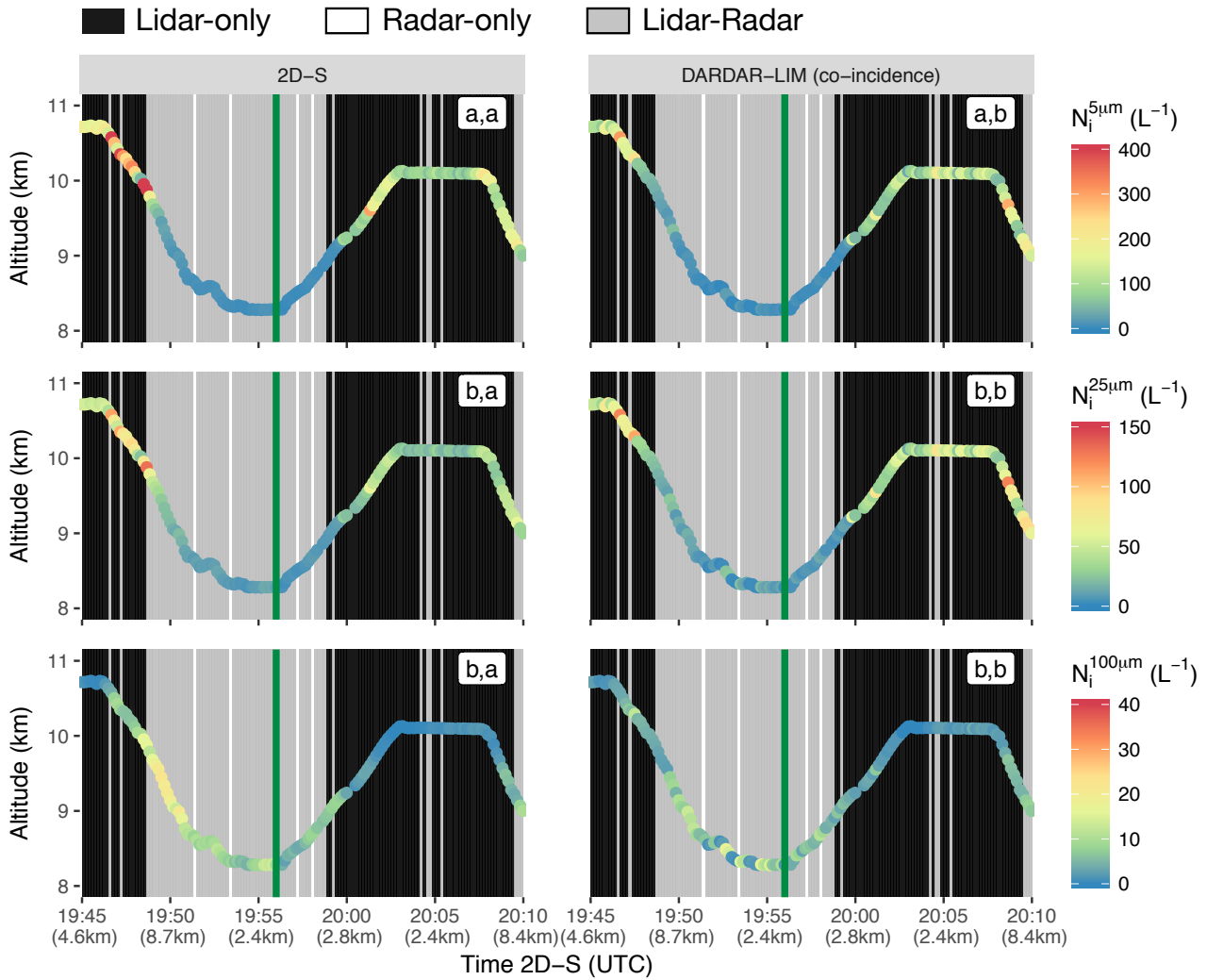Figure S6: Similar to Fig. 4 of the paper, but the histograms are separated per instrumental conditions.

Figure S7: N_i measured by the 2D-S (first column) and retrieved by DARDAR-Nice (second column) along a projection of the Learjet-25 track on the A-Train overpass, show in Fig. 5(a-b) and Fig. 6 of the paper. The N_i is provided as function of the aircraft flight time (x-axis), with the distance to the satellite overpass track indicated in brackets. The overpass time (about 19:56 UTC) is shown by a vertical green line. The color background indicates if the DARDAR-Nice N_i has been estimated under lidar-only (black), radar-only (white) or lidar-radar (grey) conditions.
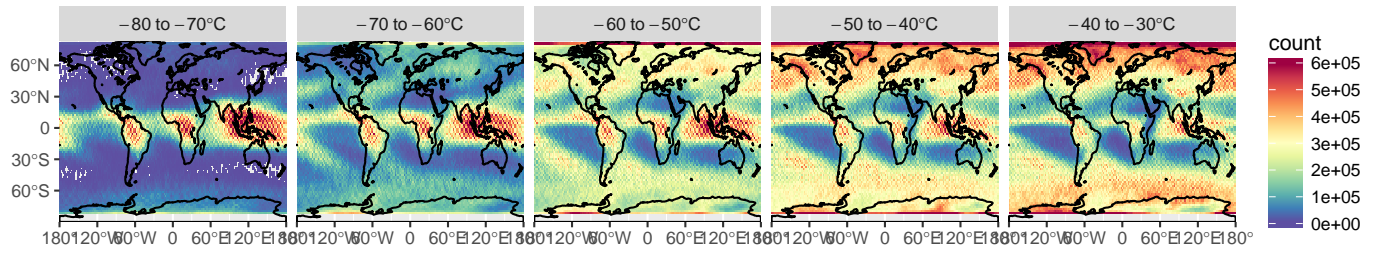
Figure S8: Spatial distribution of the count of N_i retrievals by DARDAR-Nice per temperature bin, corresponding to Fig. 7 of the paper.
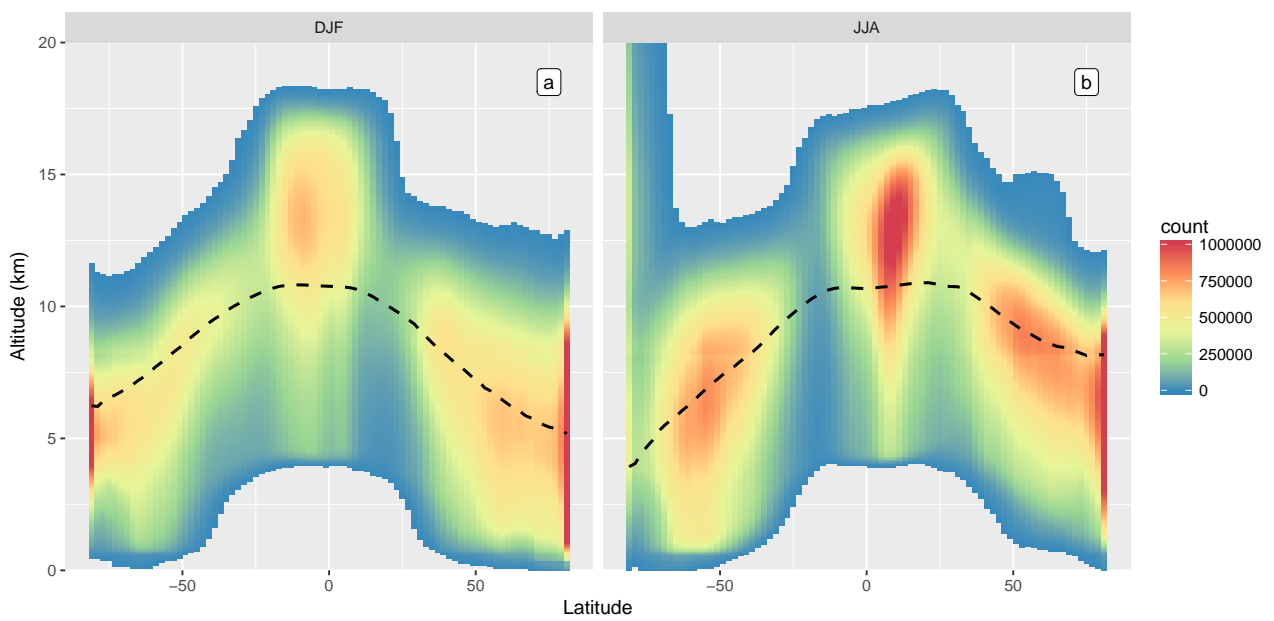
Figure S9: Spatial distribution of the count of N_i retrievals by DARDAR-Nice per temperature bin, corresponding to Fig. 9 of the paper.

References:

J. Delanoë, A. J. Heymsfield, A. Protat, A. Bansemer, and R. J. Hogan. Normalized particle size distribution for remote sensing application. *J. Geophys. Res*, 119(7):4204–4227, 2014. doi: 10.1002/2013JD020700. URL `http://dx.doi.org/10.1002/2013JD020700`.